A&A, 693, A142 (2025)
https://doi.org/10.1051/0004-6361/202451924

Astronomy & Astrophysics

A new look at the extragalactic very high energy sky: Searching for TeV-emitting candidates among the X-ray-bright, non-Fermi-detected blazar population

Stefano Marchesi[1,2,3,⋆], Antonio Iuliano[4], Elisa Prandini[5], Paolo Da Vela[2], Michele Doro[5], Serena Loporchio[6,7], Davide Miceli[5], Chiara Righi[8], Roberta Zanin[9], Ettore Bronzini[1,2], and Cristian Vignali[1,2]

[1] Dipartimento di Fisica e Astronomia (DIFA) Augusto Righi, Università di Bologna, via Gobetti 93/2, 40129 Bologna, Italy
[2] INAF-Osservatorio di Astrofisica e Scienza dello Spazio (OAS), via Gobetti 93/3, 40129 Bologna, Italy
[3] Department of Physics and Astronomy, Clemson University, Kinard Lab of Physics, Clemson, SC 29634, USA
[4] Sezione INFN di Napoli, Complesso universitario di Monte S. Angelo ed. 6 via Cintia, 80126, Napoli, Italy
[5] INFN Sezione di Padova and Università degli Studi di Padova, Via Marzolo 8, 35131 Padova, Italy
[6] Dipartimento Interateneo di Fisica, Politecnico di Bari, via Amendola 173, 70125 Bari, Italy
[7] Sezione INFN di Bari, via Orabona 4, 70125, Bari, Italy
[8] INAF – Osservatorio Astronomico di Brera, Via E. Bianchi 46, 23807 Merate, Italy
[9] Cherenkov Telescope Array Observatory gGmbH, Via Piero Gobetti, 93/3, 40129 Bologna, Italy

Received 19 August 2024 / Accepted 23 October 2024

ABSTRACT

We present the results of a multiwavelength study of blazars selected from the fifth ROMABZCAT catalog. We selected from this sample a subsample of 2435 objects that have at least one counterpart in one of the three main archival X-ray catalogs, namely the fourth release of the *XMM-Newton* Survey Science Catalogue, the second release of the *Chandra* Source Catalog, and the second *Swift* X-ray Point Source catalog of detections by *Swift-XRT*, or in the recently released eROSITA-DE Data Release 1 catalog. We first searched for different multiwavelength trends between sources with a γ-ray counterpart in the *Fermi*-LAT 14-year Source Catalog (4FGL–DR4) and sources lacking one. We find that the non-4FGL sources are on average fainter both in the X-rays and in the radio with respect to the 4FGL-detected ones, but that the two samples have similar X-ray-to-radio flux ratios and synchrotron peak frequencies. We then focused on the 1007 non-γ-ray detected population to determine whether or not there is a sample of X-ray sources that could be TeV emitters. We find that a large number of sources – mostly BL Lacs or BL Lacs with host-galaxy contribution to the spectral energy distribution – have a large synchrotron peak frequency and a large X-ray-to-radio flux ratio, two properties that characterize the vast majority of known TeV emitters. With respect to these known TeV emitters, our targets have X-ray fluxes that are about one order of magnitude fainter. We then computed the 0.2–12 keV and 20 GeV–300 TeV fluxes for the known 5BZCAT TeV emitters, and find a direct correlation between X-ray and TeV fluxes in the BL Lacs population. We used this trend to estimate the VHE flux of our targets, and find a promising sample of sources for follow-up observations with current or future, more sensitive Cherenkov telescopes; first and foremost the Cherenkov Telescope Array Observatory.

Key words. catalogs – virtual observatory tools – BL Lacertae objects: general – quasars: supermassive black holes – gamma rays: galaxies

1. Introduction

Blazars are accreting supermassive black holes (SMBHs), or active galactic nuclei (AGN), whose relativistic jets are pointed in the direction of the observer. This causes "Doppler boosting", which is a significant enhancement of the source luminosity due to the relativistic speed of the particles causing the emission. The spectral energy distribution (SED) of blazars is characterized by two clear bumps (e.g., Abdo et al. 2010): the first one at lower frequencies or energies, the so-called synchrotron peak, where the synchrotron emission is caused by the relativistic electrons in the jets; and the second at higher frequencies or energies, the "inverse Compton" peak, which is instead caused by the interaction and subsequent up-scattering in frequency of the synchrotron-produced photons with the same relativistic electrons (in the so-called synchrotron self-Compton scenario; e.g., Kirk et al. 1998).

The frequency of these two peaks can vary significantly depending on several parameters, most prominently the luminosity of the blazars and their class (e.g., Padovani & Giommi 1995; Ghisellini et al. 1998; Giommi et al. 1999; Prandini & Ghisellini 2022). For example, the synchrotron peak can be found at frequencies as low as $\nu_{\rm synch} = 10^{12}$ Hz, which is in the far-infrared band (e.g., Chen et al. 2009), and as high as $\nu_{\rm synch} = 10^{18}$ Hz, which is in the X-ray band (conventionally, between 0.1 and several hundred keV; see, e.g., Chang et al. 2019).

The X-ray band, in particular, is a key region of the blazar SED. In the most luminous and powerful blazars, most of which are detected at redshifts of $z > 1$, X-ray observations are needed to detect and constrain the shape of the rising part of the inverse Compton bump (e.g., Tavecchio et al. 2000; Sbarrato et al. 2015; Marcotulli et al. 2017; Ghisellini et al. 2019; Marcotulli et al. 2020). In a specific class of sources, aptly named high-synchrotron peaked (HSPs; also defined as

⋆ Corresponding author; stefano.marchesi@inaf.it

HBLs) blazars (e.g., Massaro et al. 2011b; Arsioli et al. 2015; Chang et al. 2017, 2019), the X-ray band is the region where the synchrotron peak is located, as mentioned above. In these extreme objects, the observational evidence supports a scenario where the X-ray emission is correlated with the very high energy (VHE; conventionally, this means that photons with energies of greater than 50 GeV have been detected) emission. For example, Massaro et al. (2011b,a) showed that known VHE emitters tend to preferentially lie in a well-defined region of diagram reporting the synchrotron peak energy versus the X-ray spectral curvature around the peak (as defined, e.g., in Tramacere et al. 2007; Massaro et al. 2008; Tramacere et al. 2011).

As a consequence of this correlation, previous works have focused on using the X-ray emission of blazars to select promising VHE emitters. This is often done by combining the X-ray information with information from at least another band (such as the infrared band – see, e.g., Massaro et al. 2013; Giommi et al. 2024, or the radio band – see, e.g., Bonnoli et al. 2015). So far, however, the overwhelming majority of the sources analyzed in these works were known γ-ray emitters, and in particular were sources detected by the *Fermi* Large Area Telescope (LAT). Indeed, predictions for detections of extragalactic sources in VHE surveys fairly often use as a starting point extrapolations based on *Fermi*-LAT luminosity functions in the MeV to GeV band. While this is certainly a tested and reliable method to estimate VHE fluxes, it could nonetheless miss a population of sources undetected in the γ-ray band and still visible at larger energies. Within this framework, we present a multiwavelength study of a broad sample of radio-selected blazars, with a specific focus on a sample of sources that lack *Fermi*-LAT data while at the same time being detected in the X-rays.

The work is organized as follows: in Section 2 we present the sample used in this work and the different multiwavelength catalogs used in our analysis. In Section 3, we analyze the multiwavelength properties of our targets, and in particular we compare the sources with a *Fermi*-LAT counterpart with those without one. In Section 4, we then use the multiwavelength properties of the non-*Fermi*-LAT detected sources, and in particular their X-ray flux, to make predictions as to their TeV emission. We finally summarize the main results of this work and discuss possible future developments in Section 5. Throughout this work, we assume a flat ΛCDM cosmology with $H_0 = 69.6\,\mathrm{km\,s^{-1}\,Mpc^{-1}}$, Ω_m=0.29, and Ω_Λ=0.71 (Bennett et al. 2014). Errors are quoted at the 90% confidence level unless otherwise stated.

2. Sample selection

All the sources analyzed in this work were initially selected from the fifth ROMABZCAT – Roma–BZCAT Multi-Frequency Catalog of Blazars (5BZCAT; Massaro et al. 2015). This catalog contains coordinates and multifrequency data for 3561 sources that are either confirmed blazars or have multiwavelength properties that strongly support a blazar nature. All the objects in the sample have a radio band detection. As reported in the description of the 5BZCAT catalog[1], each 5BZCAT source is classified in one of the four following categories based on its multiwavelength properties.

1. 5BZB: These are BL Lac objects, and, more specifically, AGNs with a featureless optical spectrum, or with only absorption lines of galactic origin and weak and narrow emission lines.
2. 5BZG: These are sources usually reported as BL Lac objects in the literature but with a SED with a significant dominance of the galactic emission over the nuclear emission. Before including a source in a follow-up analysis designed to further our understanding the appearance of its SED in the TeV band, we need to ensure that the SED emission is not significantly contaminated by the host or, in the X-ray band, by non-jet emission. While this should not be a problem for BZB sources, in BZGs the emission from the optical to the X-ray band could be significantly affected by non-jet processes, which in turn would make both the X-ray to radio flux ratio and the synchrotron peak measurements unreliable. In this regard, a specific class of sources stands out the most: clusters of galaxies whose radio and X-ray properties can in many cases be similar to those of the BZG sources. For example, Green et al. (2017) reported a list of 41 BZGs whose properties (most importantly, the presence of extended emission in the X-rays and the fraction of polarization in the radio) indicate that the emission of these sources is dominated by the cluster. We thus exclude these 41 objects from our analysis.
3. 5BZQ: These sources are flat-spectrum radio quasars (FSRQs) with an optical spectrum showing broad emission lines and dominant blazar characteristics.
4. 5BZU: These are blazars of uncertain type (BCU), and this label is adopted for a small number of sources with peculiar characteristics (e.g., sources that have been observed to be transitioning from a FSRQ state to a BL Lac one, or vice versa) but nonetheless exhibiting blazar activity.

We cross-matched the 5BZCAT with the *Fermi*-LAT 14-year Source Catalog (hereafter 4FGL-DR4, Abdollahi et al. 2022; Ballet et al. 2023), which contains 7194 γ-ray sources – 5788 of which are classified as point-like – that have been detected in 14 years of observations in the 50 MeV–1 TeV energy range with the *Fermi*-LAT. To this end, we performed a positional cross-match between the 5BZCAT coordinates and the coordinates reported as "counterpart coordinates" in the 4FGL–DR4 catalog, because the accuracy of these latter coordinates, which come from a radio, optical, or X-ray catalog, is much higher than the those of the *Fermi*-LAT sources themselves. We find a *Fermi*-LAT counterpart for 1772 5BZCAT sources, while the remaining 1748 do not have one. The median separation between the 5BZCAT sources and the 4FGL-DR4 counterparts is 0.11″, and 1725 out of 1772 objects (i.e., 97% of the 4FGL–DR4 sources) have a positional separation of smaller than 2″. We note that such a small separation is a direct consequence of the fact that the counterpart coordinates reported in the 4FGL-DR4 catalog are always the most accurate available; in the vast majority of cases, such coordinates coincide almost exactly with the 5BZCAT ones.

For the most part, the remaining sources that have a separation of larger than 2″ have a 4FGL-DR4 counterpart positional uncertainty of between 16 and 32″: these counterparts are generally RX sources detected by the ROSAT all-sky X-ray telescope (Voges et al. 1999), or are NVSS sources detected by the National Radio Astronomy Observatory (NRAO) Very Large Array (VLA) Sky Survey (Condon et al. 1998). Thus, the separation between the 5BZCAT source and the 4FGL–DR4 counterpart is well within the 4FGL–DR4 counterpart positional uncertainty.

[1] https://heasarc.gsfc.nasa.gov/w3browse/all/romabzcat.html

2.1. X-ray counterpart identification

As discussed in Sect. 1, the purpose of the present work is to understand whether or not among the blazars not detected by *Fermi*-LAT there is a population of TeV-emitting sources that could be detected by current or future Cherenkov telescopes. To test this possibility, we focus on the X-ray-detected blazars, as X-ray emission can be an effective tracer of the TeV emission, as already discussed in Sect. 1. In the following subsections, we briefly present the X-ray telescopes and catalogs that we use in this paper.

2.1.1. *XMM-Newton* and the 4XMM-DR13 catalog

The *XMM-Newton* telescope was launched on December 10, 1999, and has been operational since February 2000. *XMM-Newton* combines an excellent effective area in the 0.2–12 keV band, a large (∼30′ diameter) field of view, and a good angular resolution (∼5″ on-axis point-spread function, PSF). For this work, we use the most recent release of the *XMM-Newton* Survey Science Catalogue, 4XMM-DR13[2] (Traulsen et al. 2020; Webb et al. 2020). As reported on the 4XMM webpage, the 4XMM-DR13 catalog is generated using 13 243 *XMM-Newton* EPIC observations, covering an energy interval from 0.2 keV to 12 keV. These observations were made between 2000 February 3 and 2022 December 31. 4XMM-DR13 contains 656 997 unique sources detected over an area of ∼1328 deg^2. The median 0.2–12 keV flux of the 4XMM-DR13 population is $\sim 2.2 \times 10^{-14}$ erg s^{-1} cm^{-2}; the median positional accuracy is ∼1.57″.

For each source, a wide variety of parameters is reported, among which we mention its coordinates; count rates; fluxes and hardness ratios in different bands; the number of times the source has been observed by *XMM-Newton*; and its variability significance. The full list of parameters available for each source can be found on the dedicated webpage[3]. There are 313 5BZCAT sources (i.e., ∼9% of the whole 5BZCAT sample) with a 4XMM-DR13 counterpart within 10″.

2.1.2. *Chandra* and the 2CSC catalog

The *Chandra* telescope was launched on July 23, 1999. *Chandra* covers the 0.3–7 keV energy range and is the only X-ray instrument with a subarcsecond on-axis angular resolution (PSF∼0.5″). The field of view of its ACIS-I array is 16.9′ × 16.9′. The most recent release of the *Chandra* Source Catalog, CSC version 2.0.1[4] (hereafter 2CSC), was released on November 24, 2020 (Evans et al. 2020). This catalog contains 317 167 unique sources detected over an area of ∼560 deg^2: similarly to the *XMM-Newton* catalog, the information on multiple parameters is reported for each source.

There are 218 5BZCAT sources (i.e., ∼6% of the whole 5BZCAT sample) with a 2CSC counterpart within 5″: with respect to *XMM-Newton*, we chose to use this more conservative maximum separation, given *Chandra*'s much higher angular resolution. For the purposes of this work, we rescaled the *Chandra* 0.5–7 keV fluxes to the 0.2–12 keV band used in the *XMM-Newton* catalog using an average value that takes into account the fact that FSRQs and low- and intermediate-energy peaked BL Lacs have a typical X-ray photon index of Γ_X ∼1.6 and a flux correction factor of $k_{corr}=f_{0.2-12keV}/f_{0.5-7keV}$ = 1.5 (see, e.g., Langejahn et al. 2020; Middei et al. 2022), while high-energy-peaked BL Lacs typically have a steeper photon index of Γ_X ∼2.5 and k_{corr} = 1.7 (see, e.g., Middei et al. 2022). The *Chandra* to *XMM-Newton* flux correction factor we used is thus k_{corr}=1.6. In Section 2.2, we report the number of sources detected by both *Chandra* and *XMM-Newton*.

2.1.3. *Swift-XRT* and the 2SXPS catalog

The Neil Gehrels *Swift* Observatory was launched on November 20, 2004, and its three different telescopes observe the sky in the optical and ultraviolet (Ultraviolet/Optical Telescope, or UVOT), in the hard X-rays (14–195 keV; Burst Alert Telescope, or BAT), and in the soft X-rays (0.2–10 keV; X-ray Telescope, or XRT). The XRT has an on-axis angular resolution of ∼18″ and a 23.6 × 23.6 arcmin^2 field of view. For this work, we use the second *Swift* X-ray Point Source (2SXPS) catalog of detections by *Swift-XRT* used in photon counting (PC) mode in the 0.3–10 keV energy range. The 2SXPS catalog[5] is based on observations performed by *Swift-XRT* between January 1, 2005, and August 1, 2018; it covers an area of 3790 deg2 and contains 206 335 unique sources.

There are 1666 5BZCAT sources (i.e., ∼47% of the whole 5BZCAT sample) with a 2SXPS counterpart within 10″. Of these, 1191 also have a 4FGL-DR4 counterpart, while 475 are X-ray only sources. We rescale the 0.3–10 keV flux in the 2SXPS catalog to the 0.2–12 keV band using a correction factor of $k_{corr}=f_{0.2-12keV}/f_{0.3-10keV}$ = 1.13, which is computed assuming a photon index of Γ_X ∼2, following an approach consistent with that discussed for *Chandra*.

2.1.4. eROSITA and the eROSITA-DE Data Release 1 catalog

eROSITA (extended ROentgen Survey with an Imaging Telescope Array Predehl et al. 2021) is an X-ray telescope mounted on the Spektrum Roentgen Gamma (SRG) orbital observatory (Sunyaev et al. 2021), and covers the 0.2–8 keV energy range, albeit with a significant decline in effective area at energies of >2.3 keV. SRG was launched on July 13, 2019. eROSITA is a whole-sky survey instrument: however, in the present work, we make use of the eRASS1 catalog (Merloni et al. 2024) of the western hemisphere (which is 359.9442>GAL_LONG>179.9442 in Galactic coordinates), which is based on data taken in the first six months of eROSITA observations, which were completed in June 2020.

As eROSITA is more sensitive at lower energies, while its effective area sharply declines at energies of ≳3 keV, the eRASS1 band of reference for the flux computation is the 0.2–2.3 keV one. For the purposes of the present work, the 0.2–2.3 keV fluxes were therefore rescaled to the 0.2–12 keV ones by assuming a simple power-law model with a photon index of Γ=2, which corresponds to a flux correction factor of $k \sim 1.76$.

The 5BZCAT contains 1608 blazars[6] in the 20 627 deg^2 footprint of eRASS1. For consistency with the approach used in searching for counterparts in the other X-ray catalogs, we ran a cross-match analysis with 10″ maximum separation. We find

[2] http://xmmssc.irap.omp.eu/Catalogue/4XMM-DR13/4XMM_DR13.html
[3] http://xmmssc.irap.omp.eu/Catalogue/4XMM-DR13/4XMM-DR13_Catalogue_User_Guide.html
[4] http://cda.cfa.harvard.edu/cscweb/index.do
[5] https://heasarc.gsfc.nasa.gov/W3Browse/swift/swift2sxps.html
[6] Four additional sources (5BZG J0439+0520, 5BZG J1108–0149, 5BZG J1119+0900, and 5BZG J1445+0039) are in the sample of misclassified clusters reported in Green et al. (2017) and are thus not included in our analysis.

Table 1. Summary of 5BZCAT sources detected in different catalogs of X-ray sources.

Catalog	X-ray instrument	Area covered (deg^2)	Sources	With *Fermi*-LAT	Without *Fermi*-LAT
4XMM-DR13	*XMM-Newton*	1328	313	181 (58%)	132 (42%)
2CSC	*Chandra*	560	218	131 (60%)	87 (40%)
2SXPS	*Swift-XRT*	3790	1666	1191 (71%)	475 (29%)
eRASS1	eROSITA	20 627	1379	726 (52%)	653 (48%)
NuBlazar	*NuSTAR*	6	114	88 (77%)	26 (23%)
4XMM-DR13 or 2CSC			464	271 (58%)	193 (42%)
2SXPS, no 4XMM or 2CSC			1347	968 (72%)	379 (28%)
eRASS1 only			624	189 (30%)	435 (70%)
Overall			2435	1428 (59%)	1007 (41%)
Of which in TeVCAT			77	77 (100%)	0 (0%)

Notes. For each catalog, or combination of catalogs, we also report the number of sources with and without a counterpart in the *Fermi*-LAT 4FGL-DR4 catalog of sources detected in the 50 MeV–1 TeV energy range.

that 1379 sources out of 1608 have an eROSITA counterpart (i.e., ∼39% of the whole 5BZCAT sample). The median offset between the 5BZCAT and eROSITA positions is ∼2.6″). As a reference, in Gatuzz et al. (2024), which makes use of the eROSITA catalog of blazars that has yet to be released, the maximum separation radius between the eROSITA position and that of 5BZCAT is 8″.

When breaking down the sample of 1379 5BZCAT sources with an eROSITA counterpart into classes, we obtain the following distribution: 812 BZQs; 415 BZBs; 69 BZGs; and 83 BZUs. As a reference, Gatuzz et al. (2024) state that the eRASS1 blazar catalog (Hammerich et al., in prep.) will include 843 FSRQs and 666 BL Lacs.

We then performed a further cross-match, this time focusing on the non-4FGL subsample: we matched the 653 eROSITA sources with the 572 sources with archival X-ray data. We break down our step-to-step approach to determine how many eRASS1 sources have a counterpart in one of the other X-ray archival catalogs used in this work:

1. First, we find that 247 out of 572 sources with archival X-ray data and without a 4FGL counterpart lie in the western half of the eROSITA sky and thus can in principle have a counterpart in the eRASS1 catalog.
2. For the vast majority of these non-4FGL sources with available archival X-ray observations (218 out of 247, ∼88%), we find a counterpart in the eRASS1 catalog.
3. The 29 remaining sources that are in at least one archival catalog but not in the eROSITA one are mostly faint sources, with a median 0.2–12 keV flux $f_{0.2-12\mathrm{keV}}$=2.4 × 10^{-13} erg s^{-1} cm^{-2}; only seven sources have $f_{0.2-12\ \mathrm{keV}}$>5 × 10^{-13} erg s^{-1} cm^{-2}. This provides us with a reasonable explanation of their non-detection in eRASS1.
4. Finally, 435 objects are in the eROSITA catalog but are not in the archival sample, and can thus be defined as "eRASS1 only" sources; they are labeled as such in Table 1. The vast majority of the non-4FGL, eRASS1-only blazars are BZQs (341); 52 are BZBs, 21 BZGs, and 21 BZUs.

2.1.5. *NuSTAR* and the Nublazar catalog

The *NuSTAR* telescope (Harrison et al. 2013) was launched on June 13, 2012, and is the first telescope to focus photons at energies above 10 keV. *NuSTAR* covers the 3 to 79 keV energy range, has a ∼13′×13′ field of view, and an angular resolution of ∼58″ (half power diameter). Given its limited field of view, *NuSTAR* is mostly used as a follow-up instrument of known sources rather than as a survey instrument, although *NuSTAR* surveys of several known fields have been taken across the years (e.g., COSMOS, Civano et al. 2015; the Extended *Chandra* Deep Field South, Mullaney et al. 2015; and the North Ecliptic Pole time-domain field, Zhao et al. 2021, 2024)

Since its launch, *NuSTAR* has targeted a significant number of blazars: for this work, we use the NuBlazar catalog (Middei et al. 2022) as a reference, which contains 126 blazars observed by *NuSTAR* between its launch and September 30, 2021. Several blazars in the catalog have been observed with *NuSTAR* more than once, and the catalog contains the properties of 253 different *NuSTAR* exposures. Of these 126 blazars, 114 are reported in the 5BZCAT: all of them are also reported in at least one of the 0.3–10 keV catalogs we present in the previous paragraphs. Of 114 sources, 88 have a 4FGL–DR4 counterpart, while 26 do not have one. In the remainder of this work, we always include the *NuSTAR* information, when available, when analyzing the SEDs of our sources.

2.2. Summary of the X-ray counterparts of the 5BZCAT sources

Table 1 reports the number of sources detected in each of the five X-ray catalogs, and in selected combinations of the five, as well as the fraction of objects that have or lack a counterpart in the *Fermi*-LAT 4FGL-DR4 catalog. Overall, 2435 5BZCAT sources (i.e., ∼68% of the whole 5BZCAT sample) have at least one X-ray counterpart: of these, 1428 also have a γ-ray counterpart in the 4FGL-DR4 catalog, while the remaining 1007 do not have one. We note that the excellent positional accuracy of the 5BZCAT sources ensures that every 5BZCAT source is uniquely associated to a single X-ray object, and that there are no occurrences of multiple radio sources cross-matched to the same X-ray target. For this same reason, we expect the number of spurious associations to be small. Ajello et al. (2020) reported that the expected false-positive-counterpart rate for the 4FGL AGN population is 1.6%, which means that only about 23 objects out of 1428 might be incorrectly associated. We expect this fraction to be a good proxy for the 1007 5BZCAT sources with no 4FGL counterpart as well. In fact, blazars are rare objects both in the

radio and in the X-ray band, with number densities of $\lesssim$1 even at the faintest X-ray fluxes and radio flux densities probed in this work (see, e.g., Padovani & Giommi 1995, and Figures 4 and 5 in Padovani et al. 2007)). This, combined with the excellent positional accuracy provided by both the radio and the X-ray observations, as discussed in the previous sections, allows us to safely assume a false-positive counterpart rate of <2% (i.e., <20 sources) for the non-4FGL sample.

In the first part of this work, we focus on the subsample of 464 sources among the 2435 5BZCAT objects with at least one X-ray counterpart reported in either the *XMM-Newton* or in the *Chandra* source catalogs: specifically, 67 sources have been observed by both *Chandra* and *XMM-Newton*; 246 only by *XMM-Newton*; and 151 only by *Chandra*. Of these 464 sources, 271 (58%) have a 4FGL-DR4 counterpart, while 193 (42%) do not have one. In Section 3.1, we use this subsample of sources – which are also, on average, the targets with the best multiwavelength coverage – to get a first understanding of the parameter space covered by the non-4FGL[7] population with respect to the 4FGL one. Later in the paper, in Section 3.3, we then include the 814 non-4FGL sources with an X-ray counterpart in either the 2SXPS or the eRASS1 catalog in our analysis.

2.3. The TeVCAT catalog

The TeVCAT–TeV Gamma-Ray Source Catalog[8] (Wakely & Horan 2008) is a constantly updated online catalog of known VHE objects, that is, sources detected at energies with E$\gtrsim$50 GeV. As of May 7, 2024, 77 5BZCAT sources were reported in the TeVCAT, all of which are also reported in the 4FGL-DR4 catalog. Of these, 72 have a redshift measurement. In the remainder of this paper, we systematically compare the properties of the sources in our sample to those of the known TeV emitters.

3. Multiwavelength properties of the X-ray-detected 5BZCAT sources

In this section, we initially study the multiwavelength properties of the 464 sources that are reported in either the *XMM-Newton* or in the *Chandra* source catalogs, and in particular we compare the subsample of 271 sources with a *Fermi*-LAT 4FGL counterpart with the 193 sources without one. The purpose of this first comparison is to understand whether or not within the non-γ-ray population there are sources whose properties make them good candidates for a detection in the TeV band.

Figure 1 shows the distributions of four parameters as a function of redshift for the 464 sources mentioned above.

1. R-band magnitude (top left panel; from the 5BZCAT).
2. 1.4 GHz flux density (top right panel; from the 5BZCAT).
3. 0.2–12 keV flux (bottom left panel; from the 4XMM and 2CSC catalogs).
4. Synchrotron peak frequency (bottom right panel). This parameter has been computed using the VOU-BLazars tool (Chang et al. 2020), which allows one to quickly generate the SED of a given source, and the BlaST (Blazar Synchrotron Tool; Glauch et al. 2022), which is a deep neural network-based tool developed by Lakshminarayanan et al. (2016) that can be used to estimate the frequency of the synchrotron peak in a blazar SED.

[7] Hereafter, when we talk about 4FGL or non-4FGL samples, we are implicitly referring to the 4FGL–DR4 catalog.

[8] https://heasarc.gsfc.nasa.gov/w3browse/all/tevcat.html

We note a main trend in the plots showing the brightness of the sources at different wavelengths: the non-4FGL-detected sources tend to be slightly fainter than the 4FGL ones, although this difference is more prominent in certain regions of the electromagnetic spectrum than in others. In the optical band (Figure 1, top left panel), for example, we observe only a mild difference between the two samples. The 4FGL-detected population has a median magnitude of $R_{AB,4FGL}$ = 17.6, with the first and third quartiles of the population lying within R_{AB} = 16.1 and R_{AB} = 18.7, while the non-4FGL sample has $R_{AB,no-4FGL}$ = 18.2 with the first and third quartile of the population lying within R_{AB} = 16.8 and R_{AB} = 19.4. In the interest of readability, in the remainder of the text, we report the first and third quartile values of a parameter between square brackets, as follows: $R_{AB,no-4FGL}$ = 18.2 [16.8–19.4].

A more prominent discrepancy is instead observed in the radio part of the SEDs. In the 1.4 GHz band (Figure 1, top right panel), the median flux density of 4FGL-detected sources is $f_{1.4GHz,4FGL}$ = 345 [59–1468] mJy. The median flux density of non-4FGL-detected sources is instead $f_{1.4GHz,no-4FGL}$ = 163 [45–472] mJy. Thus, the high-radio-flux-density end of the overall sample is dominated by the 4FGL-detected sources.

Finally, in the 0.2–12 keV band, the median flux of 4FGL-detected sources is $f_{0.2-12keV,4FGL} = 2 \times 10^{-12}$ [8×10^{-13}–6×10^{-12}] erg s^{-1} cm^{-2}. For the non-4FGL population, the median X-ray flux value is $f_{0.2-12keV,no-4FGL} = 6 \times 10^{-13}$ [3×10^{-13}–2×10^{-12}] erg s^{-1} cm^{-2}, meaning that the median flux value is a factor of ~4 smaller than the median X-ray flux of the 4FGL-detected subsample.

The difference in brightness between the two samples is at least partly caused by the fact that the non-4FGL-detected population includes a broader fraction of the high-z population. More specifically, the 4FGL sample median redshift is z_{4FGL} = 0.53 [0.21–0.94], while the non-4FGL-detected sample median redshift is $z_{no-4FGL}$ = 0.83 [0.32–1.92]. Notably, 84 out 134 sources at z >1 (63% of the subsample) do not have a 4FGL counterpart.

We note that, while the 4FGL sources are on average brighter in the X-ray and radio band than the non-4FGL ones, there is instead no significant evidence of a different trend in the 0.2–12 keV to 1.4 GHz flux ratio as a function of redshift: the 4FGL sample has a median ratio of $r_{X-to-Radio,4FGL}$=280 [101–2507]. The non-4FGL sample instead has $r_{X-to-Radio,no-4FGL}$=261 [84–1124]. This ratio has been applied in the past to select potential candidate TeV emitters (the so-called extreme highly peaked BL Lac objects, or EHBLs; see, e.g., Costamante et al. 2001; Bonnoli et al. 2015), because it can be a reliable indicator of a high synchrotron peak frequency (and consequently of an inverse Compton peak in the TeV range; see, e.g., Costamante et al. 2018; Foffano et al. 2019; Righi et al. 2019): we make further use of this parameter in the following sections.

Finally, and in agreement with the line of argument above regarding the use of the X-ray-to-radio-flux ratio as a proxy for the SED shape, we do not observe a clear difference in the synchrotron peak distributions, with a median of Log(ν_{Peak})=13.5 in both populations, and fairly consistent first and third quartile ranges as well: Log($\nu_{Peak,4FGL}$) = [12.7–15.7], and Log($\nu_{Peak,no-4FGL}$) = [12.8–15.1].

3.1. 4FGL versus non-4FGL multiwavelength properties by source class

To further explore the properties of our sample, we searched for different trends between the source classes reported in the 5BZCAT catalog and reported in Section 2. As shown in Table 2,

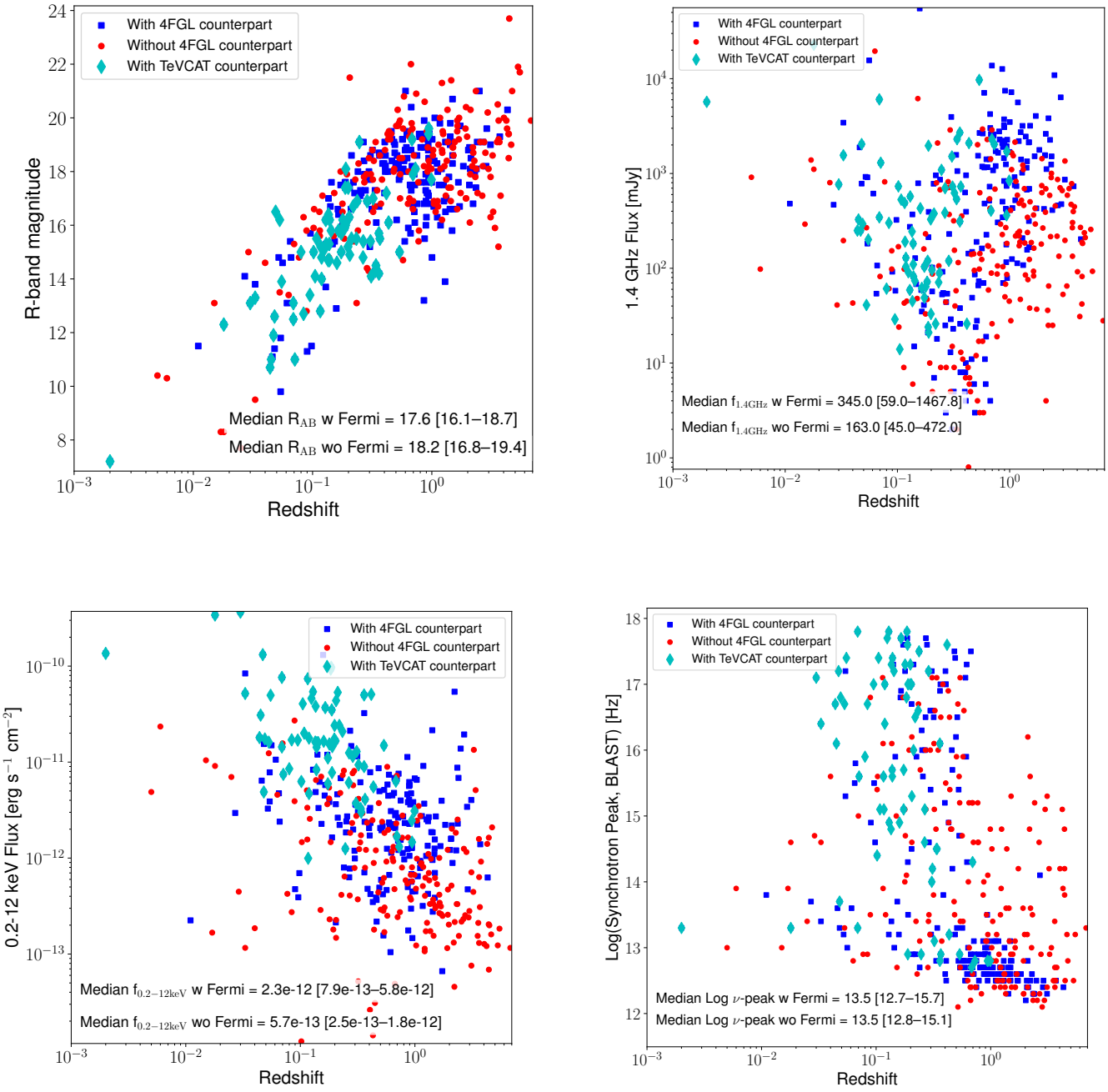

Fig. 1. R-band magnitude (top left panel), 1.4 GHz flux density (top right panel), 0.2–12 keV flux (bottom left panel), and BlaST-derived synchrotron peak frequency (bottom right panel) as a function of redshift for sources with a counterpart either in the 4XMM–DR13 catalog or in the 2CSC, with (blue squares) and without (red circles) a counterpart in the 4FGL-DR4 *Fermi*-LAT catalog. As a reference, we also include in the plot the 72 sources with redshift information and a counterpart in the TeVCAT catalog (cyan diamonds), which are therefore known TeV emitters. In the plot, we also include the median values of each parameter for both the 4FGL and the non-4FGL sample: we include in square parentheses the first and third quartiles of each subsample.

our sample contains 227 FSRQs (or BZQs in the 5BZCAT nomenclature); 143 BL Lacs (BZB); 43 BL Lacs where the SED emission shows a significant contribution from the host galaxy (BZG); and 51 blazars of uncertain type (BZU). A first thing to note is that the 4FGL and non-4FGL samples are not homogeneous in terms of the fraction of sources belonging to a given class. More specifically, 44% of the sources in the 4FGL subsample are classified as BZB, 39% as BZQ, 10% as BZU, and 8% as BZG. The non-4FGL-detected sample is instead dominated by the BZQ sources, which make up 63% of it, while the remaining 37% are divided between BZBs (13%), BZUs (12%), and BZGs (11%). This different composition of the two samples significantly contributes to their different redshift distribution, as the higher redshift population is made almost entirely of BZQs (as shown in Table 2).

As shown in Table 2, the comparison between 4FGL-detected and 4FGL-undetected sources shows that each of the four classes behaves in a way that is generally consistent with the overall population: the γ-ray population is on average brighter in both the radio and in the X-rays, while the trend is less

Table 2. Median redshift (computed on the subsample of sources with a redshift measurement), R_{AB} magnitude, 1.4 GHz flux density, 0.2–12 keV flux, and logarithm of the synchrotron peak frequency for the four classes of sources reported in 5BZCAT.

Class	N_{src}	N_{TeV}	With 4FGL-DR4 counterpart						Without 4FGL-DR4 counterpart					
			N_{src}	z	R_{AB}	$f_{1.4GHz}$ (mJy)	$f_{0.2-12keV}$ (erg s^{-1} cm^{-2})	Log(ν_{Peak}) (Hz)	N_{src}	z	R_{AB}	$f_{1.4GHz}$ (mJy)	$f_{0.2-12keV}$ (erg s^{-1} cm^{-2})	Log(ν_{Peak}) (Hz)
FSRQ (BZQ)	227 (49%)	5	105 (39%)	0.93 [0.62–1.48]	18.1 [16.9–19.0]	1151 [411–2197]	2.2×10^{-12} [$1.1–4.5]\times10^{-12}$	12.7 [12.5–12.9]	122 (63%)	1.36 [0.75–2.40]	18.3 [17.0–19.4]	232 [96–618]	5.3×10^{-13} [$2.4–14.4]\times10^{-13}$	13.1 [12.5–14.0]
BLL (BZB)	143 (31%)	27	118 (44%)	0.30 [0.17–0.45]	17.6 [16.7–19.2]	62 [12–169]	2.1×10^{-12} [$0.3–5.1]\times10^{-12}$	15.6 [14.5–16.7]	25 (13%)	0.38 [0.31–0.50]	19.4 [18.4–19.8]	12 [5–17]	3.2×10^{-13} [$1.8–7.9]\times10^{-13}$	15.9 [15.4–16.5]
BLL-host (BZG)	43 (9%)	3	21 (8%)	0.14 [0.07–0.20]	16.1 [14.0–17.5]	92 [53–324]	2.4×10^{-12} [$0.8–3.9]\times10^{-12}$	15.8 [14.6–17.2]	22 (11%)	0.12 [0.08–0.20]	16.0 [14.8–17.6]	45 [28–165]	4.4×10^{-13} [$2.3–24.2]\times10^{-13}$	15.5 [14.6–16.1]
BCU (BZU)	51 (12%)	5	27 (10%)	0.68 [0.05–0.87]	17.5 [14.0–18.9]	629 [541–3467]	4.1×10^{-12} [$2.2–8.8]\times10^{-12}$	13.0 [12.7–13.5]	24 (12%)	0.44 [0.08–0.67]	17.1 [13.5–19.2]	156 [85–829]	2.0×10^{-12} [$0.7–5.0]\times10^{-12}$	13.9 [13.0–14.9]
Overall	464	40	271	0.53 [0.21–0.94]	17.6 [16.1–18.7]	345 [59–1468]	2.3×10^{-12} [$0.8–5.8]\times10^{-12}$	13.5 [12.7–15.7]	193	0.83 [0.32–1.92]	18.2 [16.8–19.4]	163 [45–472]	5.7×10^{-13} [$2.5–18.0]\times10^{-13}$	13.5 [12.8–15.1]

Notes. The numbers in square parentheses are the first and third quartile values for each of the parameters. For each of the four classes, we further break down the sample into *Fermi*-LAT-detected and -undetected sources. N_{src} is the number of sources in each of the four classes (in parentheses, we report the fraction of sources in the class with respect to the whole population), while N_{TeV} is the number of sources with a counterpart in the TeVCAT. We also report as a reference the median values for the whole sample of 464 sources with either an *XMM-Newton* or *Chandra* counterpart.

significant in the optical band, particularly for the BZQ, BZG, and BZU populations.

Finally, BZBs, BZGs, and BZQs have similar distributions of the synchrotron peak frequency between 4FGL-detected and 4FGL-undetected sources, while we observe a different trend in the BZU population. More specifically, BZUs with a *Fermi*-LAT detection have a median synchrotron peak frequency, Log($\nu_{Peak,BZU,4FGL}$)=13.0, which is almost one order of magnitude lower than the median synchrotron peak frequency for BZUs without a *Fermi*-LAT counterpart (Log($\nu_{Peak,BZU,4FGL}$)=13.9). It is widely known that FSRQs generally peak at much lower frequencies than BL Lacs: this is clearly observable in the sample studied in this work as well, as the median synchrotron peak frequency for the 227 FSRQs in our sample is Log($\nu_{Peak,BZQ}$)=12.8, with a standard deviation of $\sigma_{Log(\nu Peak,BZQ)}$=0.8, while for the 186 sources that make up the BL Lac population (both BZB and BZG), we measure a median synchrotron peak frequency of Log($\nu_{Peak,BZB,BZG}$)=15.6, with a standard deviation of $\sigma_{Log(\nu Peak,BZB,BZG)}$=1.4. Consequently, the discrepancy we measure in the BZU population may suggest that the *Fermi*-LAT-detected sample of BZUs contains a larger fraction of FSRQs with respect to the non-LAT-detected sample.

3.2. Properties of the known TeV emitters

To further characterize the typical properties of the extragalactic population emitting in the TeV band, we use the TeVCAT (Wakely & Horan 2008). This, as mentioned earlier in the text, is a regularly updated catalog of known VHE objects, that is, of sources with a detection at energies of >50 GeV. Figure 1 the 72 sources (out of 77) in our sample that have a TeVCAT counterpart and a redshift measurement are plotted as cyan diamonds: all of them are also detected by the *Fermi*-LAT. As shown in the figure, the TeVCAT sources are located in the lower-redshift, higher-flux parameter space at all wavelengths. More specifically, in the X-ray band, all but three TeVCAT sources have 0.2–12 keV flux larger than 10^{-12} erg s^{-1} cm^{-2}. In the radio band, the TeVCAT sample covers a broader range of fluxes than in the X-rays; nonetheless, the median flux density of the TeVCAT population is $f_{1.4GHz,TeVCAT}$ = 297 mJy, which is larger than that of the sample of 1242 4FGL-detected objects with an X-ray counterpart ($f_{1.4GHz,4FGL}$ = 222 mJy). Finally, the median optical magnitude of the TeVCAT sample is R_{AB} = 15.4, which is over two orders of magnitude brighter than that of the 4FGL-detected population ($R_{AB,4FGL}$ = 17.9). We also note that the median redshift of the TeVCAT sources is z=0.16[9], and only nine sources have a redshift of z >0.4 (six of these are classified as FSRQs, two as BZUs with low synchrotron peak frequency, and only one, TeV J0507+676, is a BL Lac).

Finally, the synchrotron peak frequency distribution is shifted toward larger frequencies with respect to the overall population. More specifically, the TeVCAT subsample has a median peak frequency of Log($\nu_{Peak,TeVCAT}$)=15.9. This is consistent with the fact that the vast majority of known TeV-emitting extragalactic sources are BL Lacs rather than FSRQs. Indeed, in our sample of 77 TeVCAT-detected sources, 61 are classified as BZB, 3 as BZG, and 5 as BZU, while only 8 are classified as BZQ. These numbers do not change significantly if we extend the comparison to the whole TeVCAT sample, which as of January 2024 contains about 70 BL Lacs and only 10 BZQ sources, the latest of which – OP 313 (z=0.997) – was detected by the Large-Sized Telescope (LST)–1 in December 2023 (Cortina & CTAO LST Collaboration 2023).

3.3. 2SXPS and eRASS1 counterparts and the overall properties of the non-4FGL, X-ray detected population

To complete our analysis, and more specifically to obtain a complete census of those sources that do not have a *Fermi*-LAT-detected counterpart but are nevertheless detected in the X-rays, we include in our sample the 379 5BZCAT sources that lack a 4FGL-DR4 counterpart and have an X-ray counterpart in the *Swift-XRT* 2SXPS catalog, as well as the 435 5BZCAT sources without a 4FGL counterpart and whose only X-ray counterpart is in the eROSITA eRASS1 catalog. The vast majority of these 814 sources (611 out of 814; 75% of the 2SXPS or eRASS1-only subsample) are classified as BZQs, with 106 (13%) classified as BZBs, 55 (7%) as BZGs, and 42 (5%) as BZUs.

When combining these 814 sources with the 193 non-4FGL ones with either a 4XMM-DR13 or a 2CSC counterpart, we thus have a sample of 1007 5BZCAT sources without a 4FGL counterpart and with an X-ray detection. The sample has the following source class breakdown: 733 (73%) BZQs, 131 (13%) BZBs, 77 (8%) BZGs, and 66 (7%) BZUs.

[9] Four targets do not have a reliable redshift measurement.

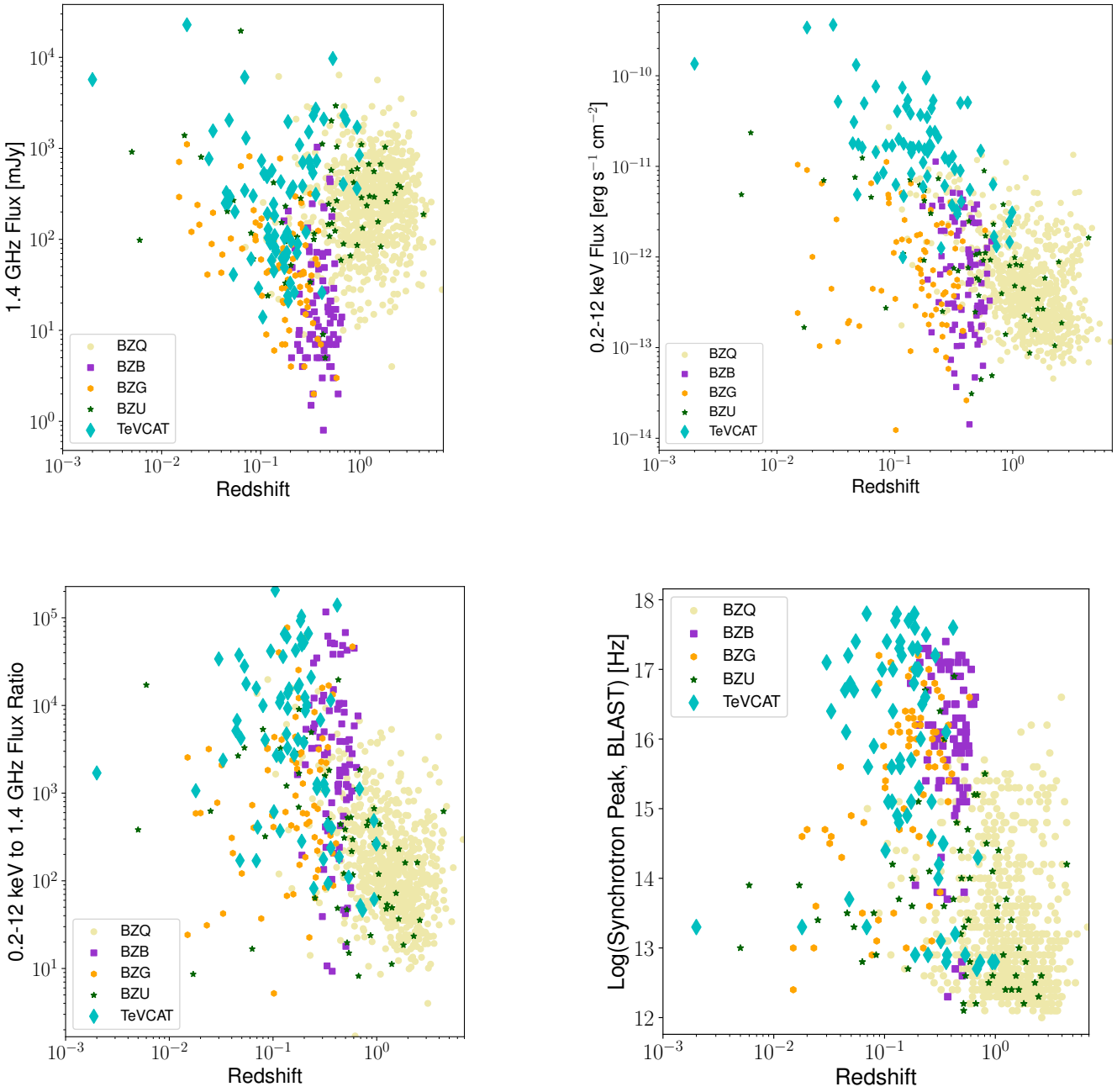

Fig. 2. R-band magnitude (top left panel), 1.4 GHz flux density (top right panel), 0.2–12 keV flux (bottom left panel), and BlaST-derived synchrotron peak frequency (bottom right panel) as a function of redshift for all the 1007 5BZCAT sources without a counterpart in the 4FGL-DR4 *Fermi*-LAT catalog and with at least one X-ray counterpart in the 4XMM–DR13, 2CSC, 2SXPS, or eRASS1 catalogs. The different markers are linked to the 5BZCAT different blazar classes: BZQs (FSRQs) are plotted as pale gold circles, BZBs (BL Lacs) as violet squares, BZGs (BL Lacs with a significant contribution to the optical and infrared emission by the host galaxy) as orange hexagons, and BZU (blazars of uncertain classification) as green stars. As a reference, we also include in the plot those sources with a counterpart in the TeVCAT catalog (cyan diamonds), which are therefore known TeV emitters.

Figure 2 shows the trend in the 1.4 GHz flux density (top left), 0.2–12 keV flux (top right), 0.2–12 keV over 1.4 GHz flux ratio (bottom left), and synchrotron peak frequency (bottom right) as a function of redshift for all the 1007 5BZCAT sources without a counterpart in the 4FGL-DR4 *Fermi*-LAT catalog and with at least one X-ray counterpart in the 4XMM–DR13, 2CSC, 2SXPS, or eRASS1 catalogs; each of these parameters has been derived in the same way, as presented in Section 3. We also report a complete breakdown of the sample properties by source class in Table 3.

When analyzing the observed 0.2–12 keV X-ray flux, we use the 4XMM–DR13 information when available (i.e., for 156 sources); otherwise we use the 2CSC information when the 4XMM–DR13 is not available (37 sources), the 2SXPS information when neither the 4XMM–DR13 nor the 2CSC information is available (379 sources), and the eRASS1 for the remaining 435 sources. As mentioned in Section 2.1, the 2CSC, 2SXPS, and eRASS1 fluxes have been rescaled to the 4XMM-DR13 0.2–12 keV band from the original 0.5–7 keV, 0.3–10 keV, and 0.2–2.3 keV bands, respectively.

Table 3. Properties of the 1007 X-ray-detected sources without a 4FGL counterpart, divided by 5BZCAT class.

Class	N_{src}	z	R_{AB}	$f_{1.4GHz}$ (mJy)	$f_{0.2-12keV}$ ($\times 10^{-13}$ erg s^{-1} cm^{-2})	$r_{X-Radio}$	Log(ν_{Peak}) (Hz)
FSRQ (BZQ)	733 (73%)	1.35 [0.88–2.10]	18.5 [17.4–19.4]	261 [119–469]	4.3 [2.3–9.2]	125 [62–341]	12.9 [12.5–13.7]
BLL (BZB)	131 (13%)	0.42 [0.32–0.50]	19.2 [18.6–19.6]	19 [7–95]	3.8 [2.1–12.1]	1760 [213–7643]	15.8 [14.3–16.5]
BLL-host (BZG)	77 (8%)	0.18 [0.10–0.27]	17.1 [14.9–18.1]	53 [24–124]	5.6 [2.4–18.3]	730 [267–3184]	15.6 [14.6–16.2]
BCU (BZU)	66 (7%)	0.53 [0.20–1.05]	18.1 [16.6–19.4]	264 [107–560]	8.0 [2.8–24.3]	296 [50–1015]	13.4 [12.7–14.2]
Overall	1007	1.12 [0.52–1.88]	18.5 [17.4–19.3]	204 [79–421]	4.5 [2.3–11.0]	170 [66–592]	13.2 [12.5–14.7]
TeV population	77	0.17 [0.10–0.27]	15.4 [14.3–16.3]	294 [82–729]	160.6 [66.1–366.5]	4737 [549–19 327]	15.8 [14.3–17.0]

Notes. We report the median value with the first and third quartile of the distribution (in square brackets) for R_{AB} magnitude, 1.4 GHz flux, 0.2–12 keV flux, 0.2–12 keV over 1.4 GHz flux ratio, and logarithm of the synchrotron peak frequency for the four classes of sources reported in the 5BZCAT. The values are computed only for the sources for which a parameter measurement is available. N_{src} is the number of sources in each of the four classes. We also report as a reference the median values for the whole sample of 1007 sources, as well as for the 77 TeVCat sources with an X-ray counterpart.

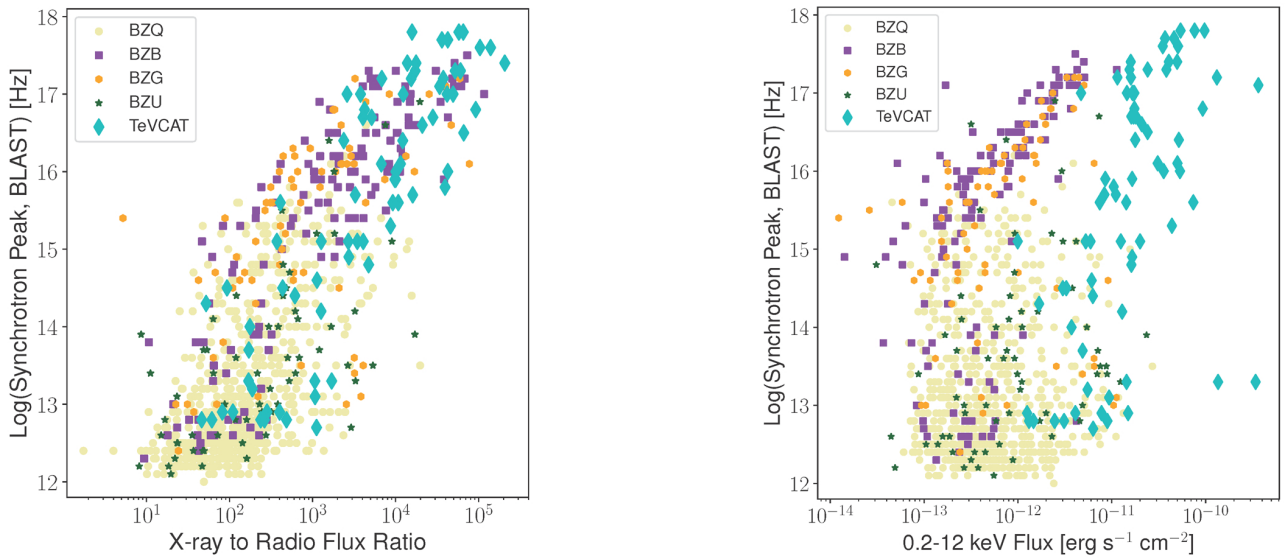

Fig. 3. BlaST-derived synchrotron peak frequency as a function of the 0.2–12 keV/1.4 GHz flux ratio (left) and of the 0.2–12 keV flux (right) for the 1007 5BZCAT sources without a *Fermi*-LAT counterpart and with an X-ray counterpart. The sources are color-coded according to class using the same coding as that described in Figure 2.

As shown in Figure 2, for all four parameters of interest, the parameter space populated by the known TeVCAT sources is also populated by a non-negligible number of targets that belong to our non-4FGL sample. In particular, two classes of sources stand out significantly when analyzing the trends in X-ray-to-radio-flux ratio as a function of redshift and with the synchrotron peak frequency: BZBs and BZGs, that is, BL Lacs sources where either the broadband SED emission is dominated by the jet emission (BZBs), or where the host galaxy emission significantly contributes to the overall SED (BZGs).

Two parameters in particular can be used to parameterize this visual evidence: the X-ray-to-radio-flux ratio, and the synchrotron peak frequency. The median X-ray-to-radio-flux ratio of the TeVCAT sample is $r_{X-Radio} = 4485$, with 55 out of 77 sources having $r_{X-Radio} > 1000$. The BZB sample has median $r_{X-Radio} = 2111$, and 54 out of 79 sources (68%) have $r_{X-Radio} > 1000$, while the BZG sample has median $r_{X-Radio} = 1084$, and 28 out of 56 sources (50%) have $r_{X-Radio} > 1000$. The TeVCAT, BZB, and BZG samples also have very similar median synchrotron peak frequencies: Log($\nu_{Peak,TeV,Hz}$) = 15.9 [14.3–17.0]; Log($\nu_{Peak,BZB,Hz}$) = 16.0 [14.3–16.5]; Log($\nu_{Peak,BZG,Hz}$) = 15.6 [14.6–16.2].

To further explore the overlap between the parameter space populated by known extragalactic TeV emitters and the X-ray-detected, non-4FGL 5BZCAT sample, the left panel of Figure 3 shows the trend with the 0.2–12 keV/1.4 GHz flux ratio of the SED synchrotron peak frequency. This plot shows even more clearly how a significant population of BZBs and BZGs lie in the same parameter space that contains the majority of the TeVCAT population, that is, at higher flux ratios and higher synchrotron peak frequencies. Specifically, 46 out of 77 TeVCAT sources (i.e., 61% of the known TeV objects) have a 0.2–12 keV/1.4 GHz flux ratio of $r_{X-Radio} > 2 \times 10^3$ and a synchrotron peak frequency of Log(ν_{Peak})>15. Also, 43 of these 46 sources are classified as BZBs, and 3 as BZGs. In this same parameter space, we have 70 5BZCAT sources that lack a 4FGL-DR4 counterpart: 41 are classified as BZB; 17 as BZG; 8 as BZQ; and 4 as BZU.

The right panel of Figure 3 also reports the trend with the 0.2–12 keV flux of the SED synchrotron peak frequency. This plot immediately clarifies why the sources we selected lack (as of today) a TeV counterpart, despite being in the same region of the X-ray-to-radio flux ratio versus synchrotron peak parameter space of the majority of the known TeV emitters. As can be seen (and as shown in the top right panel of Figure 2), the X-ray flux of

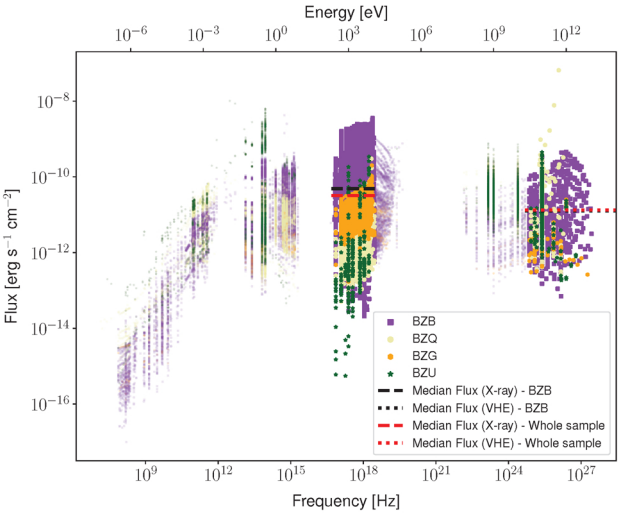

Fig. 4. Spectral energy distributions of the 77 TeVCAT sources analyzed in this work. The SEDs are color-coded by class using the same coding described in Figure 2. We also show with black (red) dashed and dotted lines the median 0.2–12 keV and 20 GeV–300 TeV fluxes of the BZB subsample (overall population).

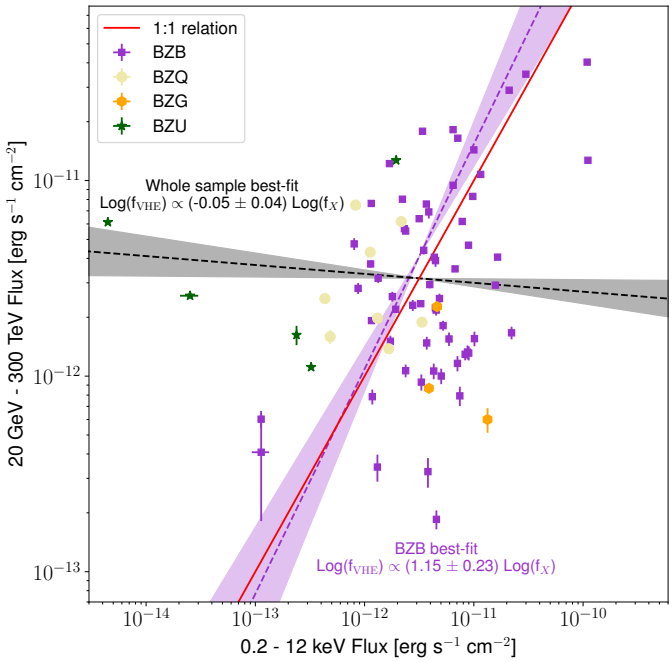

Fig. 5. Average 20 GeV–300 TeV flux as a function of the average 0.2–12 keV flux for the 77 TeVCAT sources in our sample. The data points are color-coded according to class, using the same coding as that described in Figure 2. In the plot, we also include the best-fit linear regression between the logarithm of the VHE flux and the logarithm of the X-ray flux, i.e., for the whole sample (dashed black line) and for the BZB subsample (violet dashed line). For reference, we also plot the 1:1 relation (solid black line).

our targets is systematically fainter than that of the known TeVCAT sources: more specifically, the median 0.2–12 keV flux of the TeVCAT population is 1.6×10^{-11} [6.6×10^{-12} erg s^{-1} cm^{-2} –3.7×10^{-11}] erg s^{-1} cm^{-2}, while the median 0.2–12 keV flux of the non–4FGL population is 4.5×10^{-13} [2.3×10^{-13}–1.1×10^{-12}] erg s^{-1} cm^{-2}. Table 3 shows a breakdown by source class, which shows that the median values do not change significantly among the four source classes reported in the BZCAT, with the median X-ray flux varying between 3.8×10^{-13} erg s^{-1} cm^{-2} for the BZB sample and 8.0×10^{-13} erg s^{-1} cm^{-2} for the BZU sample.

Finally, we note that Bonnoli et al. (2015) also used a selection criterion on the flux ratio to select potential VHE blazars, which is, $r_{0.1-2.4\ \mathrm{keV}/1.4\mathrm{G\ Hz}} > 10^4$. The X-ray flux they used to compute the ratio was the ROSAT 0.1–2.4 keV one (Plotkin et al. 2010); when rescaled to the 0.2–12 keV band flux used in this work, assuming a photon index of Γ=2 (as explained in Section 2.1), the threshold corresponds to $r_{0.2-12\ \mathrm{keV}/1.4\ \mathrm{GHz}} \gtrsim 1.7 \times 10^4$. This criterion is met by only 21 out of 77 TeVCAT sources (i.e., ∼27% of the sample), but is nonetheless effective in selecting a parameter space that is populated almost entirely by VHE emitters, particularly when including a secondary selection criterion based on the X-ray flux.

4. Estimating the TeV emission of the population of X-ray bright, non-Gamma-ray-detected targets

As shown in the right panel of Figure 3 and discussed in the previous section, our analysis reveals a population of sources that have multiwavelength properties consistent with those of the known TeV blazars reported in the TeVCAT, but that are generally fainter in the X-ray band. To get a first estimate of how bright these sources could be in the TeV band, we use the 77 TeVCAT sources in our sample as a reference. In Figure 4 we report the SEDs of these objects color-coded according to source class. As can be seen, the sources tend to share a similar SED shape, with the majority of the sources (with the exception of the BZQs) having a synchrotron peak frequency at energies of greater than 10^{15} Hz, as already discussed in the previous section.

When analyzing the SEDs of known VHE emitters, we are most interested in measuring fluxes in the X-rays (0.2–12 keV) and in the VHE (>20 GeV) bands in order to determine whether or not and how the two quantities are correlated. As mentioned above, the vast majority of known TeV emitters are BL Lacs (BZB in the 5BZCAT classification); more specifically, our sample contains 61 BZBs, with a median 0.2–12 keV flux value $f_X = 4.9 \times 10^{-11}$ erg s^{-1} cm^{-2}, and median VHE (20 GeV–300 TeV) flux value f_{VHE} 1.3×10^{-11} erg s^{-1} cm^{-2}. These two values are reported in Figure 4 as black dashed and dotted lines, respectively. In the same figure, we also report (as red dashed and dotted lines, respectively) the median 0.2–12 keV and 20 GeV–300 TeV for the 77 TeVCAT sources, which are $f_X = 3.2 \times 10^{-11}$ erg s^{-1} cm^{-2}, and $f_{VHE} = 1.3 \times 10^{-11}$ erg s^{-1} cm^{-2}.

To further explore the X-ray to VHE correlation, we plot in Figure 5 the average 20 GeV–300 TeV flux as a function of the average 0.2–12 keV flux for the 77 TeVCAT sources in our sample, once again color-coding them according to source class. A few trends are immediately evident: first of all, BZQs generally have VHE fluxes consistent with or, more often, larger than the X-ray ones. When performing a linear regression (in the Log-Log space) of the whole sample, we do not find a significant correlation between the two fluxes, with Log(f_{VHE}) ∝ (–0.05 ± 0.04) Log(f_X). A more prominent trend is instead observed when focusing on the BL Lac (BZB) population: in this case, while the distribution has a relatively large scatter, we measure a correlation of Log(f_{VHE}) ∝ (1.15 ± 0.23) Log(f_X), which is consistent within the uncertainties with the 1:1 trend.

This means that, at zero order, the X-ray flux can be treated as a fairly reasonable proxy of the VHE flux for BZB sources, and thus the plot shown in the right panel of Figure 3 can be

treated as a synchrotron peak versus VHE flux plot for the BZB subsample. It can then be seen that a non-negligible population of sources exist that might have VHE fluxes $\sim 10^{-12}$ erg s^{-1} cm^{-2}: these objects represent an intriguing pool of targets for dedicated observing campaigns with current facilities, such as MAGIC, HESS, VERITAS, or LST-1, and should be easily detected by future facilities such as the Cherenkov Telescope Array Observatory, whose sensitivity will improve on that of current facilities by almost one order of magnitude (Hofmann & Zanin 2023).

5. Conclusions and future developments

We analyzed a sample of 2435 blazars reported in the 5BZCAT that have an X-ray counterpart in at least one of the *XMM-Newton*, *Chandra*, *Swift-XRT*, or eROSITA point-like source catalogs, with the goal of determining whether or not X-ray emission can be used as an effective proxy to find and characterize candidate TeV-emitting blazars that would be missed by simply extrapolating the source γ-ray emission. The main results of this work can be summarized as follows:

1. We selected a sample of 464 sources with high-quality X-ray data from either *XMM-Newton* or *Chandra* observations to determine the multiwavelength properties of the sources with a γ-ray counterpart in the 4FGL-DR4 catalog. We find that the non-4FGL-detected sources are on average fainter both in the X-rays and in the radio with respect to the 4FGL-detected ones, but the two samples have similar X-ray-to-radio flux ratios and synchrotron peak frequencies. Furthermore, as shown in Figure 1, when plotting these two parameters versus redshift, a significant fraction of the non-4FGL-detected sources lie in a similar parameter space to the known TeV emitters.
2. We then focused on the 1007 non-γ-ray-detected population to determine whether or not there is a sample of X-ray sources that could be TeV emitters: for this purpose, we included in our sample also those sources detected only by *Swift-XRT*, or eROSITA. We find that a large number of sources – mostly BL Lacs or BL Lacs with a host-galaxy contribution to the SED – have a large synchrotron peak frequency ($\mathrm{Log}\nu_{\mathrm{Peak/Hz}} > 15$) and a large X-ray-to-radio flux ratio ($r_{\mathrm{X-Radio}} > 1000$), as reported both in Figure 2 and Table 3. These two properties also characterize the vast majority of known TeV emitters: however, with respect to these known TeV emitters, our targets have X-ray fluxes that are about one order of magnitude fainter.
3. Finally, we computed the 0.2–12 keV and 20 GeV–300 TeV fluxes for the known 5BZCAT TeV emitters, and find a direct correlation between X-ray and TeV fluxes in the BL Lacs population. This trend can be used to estimate the VHE flux of our targets, and to select sources for follow-up observations with current or future, more sensitive Cherenkov telescopes: first and foremost, the Cherenkov Telescope Array Observatory (Hofmann & Zanin 2023).

The sample we selected can be used for a variety of purposes. Our group is currently working on the analysis of subclasses of targets with newly developed tools that allow the SED of a blazar to be fitted with physically meaningful emission models (Iuliano et al., in prep.). We plan to test the SED fitting tool released by the Markarian Multiwavelength Data Center[10] (Sahakyan et al. 2024), which is based on a convolutional neural network (CCN) whose parameters and technical implementation are presented in Bégué et al. (2024). Additionally, with this paper, we also make available the catalog of 1007 5BZCAT sources without a 4FGL counterpart and with at least one detection in the 4XMM-DR13, 2CSC, 2SXPS, or eRASS1 catalogs: we present the properties of this catalog in the Appendix.

[10] https://mmdc.am/

Data availability

The catalog of 1007 sources without 4FGL-DR4 counterpart presented in the Appendix is available in electronic form at the CDS via anonymous ftp to cdsarc.cds.unistra.fr (130.79.128.5) or via https://cdsarc.cds.unistra.fr/viz-bin/cat/J/A+A/693/A142.

Acknowledgements. The research activities described in this paper were carried out with contribution of the Next Generation EU funds within the National Recovery and Resilience Plan (PNRR), Mission 4 – Education and Research, Component 2 – From Research to Business (M4C2), Investment Line 3.1 – Strengthening and creation of Research Infrastructures, Project IR0000012 – "CTA+ – Cherenkov Telescope Array Plus". This work makes use of Matplotlib (Hunter 2007) and NumPy (Harris et al. 2020). S.M. thanks Lea Marcotulli for the helpful suggestions on blazar source catalogs, and Marco Ajello, Mauro Dadina, and Eleonora Torresi for the useful discussions.

References

Abdo, A. A., Ackermann, M., Agudo, I., et al. 2010, ApJ, 716, 30
Abdollahi, S., Acero, F., Baldini, L., et al. 2022, ApJS, 260, 53
Ajello, M., Angioni, R., Axelsson, M., et al. 2020, ApJ, 892, 105
Arsioli, B., Fraga, B., Giommi, P., Padovani, P., & Marrese, P. M. 2015, A&A, 579, A34
Ballet, J., Bruel, P., Burnett, T. H., Lott, B., & The Fermi-LAT collaboration. 2023, arXiv e-prints [arXiv:2307.12546]
Bégué, D., Sahakyan, N., Dereli Bégué, H., et al. 2024, ApJ, 963, 71
Bennett, C. L., Larson, D., Weiland, J. L., & Hinshaw, G. 2014, ApJ, 794, 135
Bonnoli, G., Tavecchio, F., Ghisellini, G., & Sbarrato, T. 2015, MNRAS, 451, 611
Chang, Y. L., Arsioli, B., Giommi, P., & Padovani, P. 2017, A&A, 598, A17
Chang, Y. L., Arsioli, B., Giommi, P., Padovani, P., & Brandt, C. H. 2019, A&A, 632, A77
Chang, Y. L., Brandt, C. H., & Giommi, P. 2020, Astron. Comput., 30, 100350
Chen, Z., Gu, M., & Cao, X. 2009, MNRAS, 397, 1713
Civano, F., Hickox, R. C., Puccetti, S., et al. 2015, ApJ, 808, 185
Condon, J. J., Cotton, W. D., Greisen, E. W., et al. 1998, AJ, 115, 1693
Cortina, J., & CTAO LST Collaboration 2023, The Astronomer's Telegram, 16381, 1
Costamante, L., Ghisellini, G., Giommi, P., et al. 2001, A&A, 371, 512
Costamante, L., Bonnoli, G., Tavecchio, F., et al. 2018, MNRAS, 477, 4257
Evans, I. N., Primini, F. A., Miller, J. B., et al. 2020, in American Astronomical Society Meeting Abstracts, 235, 154.05
Foffano, L., Prandini, E., Franceschini, A., & Paiano, S. 2019, MNRAS, 486, 1741
Gatuzz, E., Wilms, J., Hämmerich, S., & Arcodia, R. 2024, A&A, 683, A213
Ghisellini, G., Celotti, A., Fossati, G., Maraschi, L., & Comastri, A. 1998, MNRAS, 301, 451
Ghisellini, G., Perri, M., Costamante, L., et al. 2019, A&A, 627, A72
Giommi, P., Menna, M. T., & Padovani, P. 1999, MNRAS, 310, 465
Giommi, P., Sahakyan, N., Israyelyan, D., & Manvelyan, M. 2024, ApJ, 963, 48
Glauch, T., Kerscher, T., & Giommi, P. 2022, Astron. Comput., 41, 100646
Green, T. S., Edge, A. C., Ebeling, H., et al. 2017, MNRAS, 465, 4872
Harris, C. R., Millman, K. J., van der Walt, S. J., et al. 2020, Nature, 585, 357
Harrison, F. A., Craig, W. W., Christensen, F. E., et al. 2013, ApJ, 770, 103
Hofmann, W., & Zanin, R. 2023, arXiv e-prints [arXiv:2305.12888]
Hunter, J. D. 2007, Comput. Sci. Eng., 9, 90
Kirk, J. G., Rieger, F. M., & Mastichiadis, A. 1998, A&A, 333, 452
Lakshminarayanan, B., Pritzel, A., & Blundell, C. 2016, arXiv e-prints [arXiv:1612.01474]
Langejahn, M., Kadler, M., Wilms, J., et al. 2020, A&A, 637, A55
Marcotulli, L., Paliya, V. S., Ajello, M., et al. 2017, ApJ, 839, 96
Marcotulli, L., Paliya, V., Ajello, M., et al. 2020, ApJ, 889, 164
Massaro, F., Tramacere, A., Cavaliere, A., Perri, M., & Giommi, P. 2008, A&A, 478, 395

Massaro, F., Paggi, A., & Cavaliere, A. 2011a, ApJ, 742, L32
Massaro, F., Paggi, A., Elvis, M., & Cavaliere, A. 2011b, ApJ, 739, 73
Massaro, F., Paggi, A., Errando, M., et al. 2013, ApJS, 207, 16
Massaro, E., Maselli, A., Leto, C., et al. 2015, Ap&SS, 357, 75
Merloni, A., Lamer, G., Liu, T., et al. 2024, A&A, 682, A34
Middei, R., Giommi, P., Perri, M., et al. 2022, MNRAS, 514, 3179
Mullaney, J. R., Del-Moro, A., Aird, J., et al. 2015, ApJ, 808, 184
Padovani, P., & Giommi, P. 1995, ApJ, 444, 567
Padovani, P., Giommi, P., Landt, H., & Perlman, E. S. 2007, ApJ, 662, 182
Plotkin, R. M., Anderson, S. F., Brandt, W. N., et al. 2010, AJ, 139, 390
Prandini, E., & Ghisellini, G. 2022, Galaxies, 10, 35
Predehl, P., Andritschke, R., Arefiev, V., et al. 2021, A&A, 647, A1
Righi, C., Tavecchio, F., & Pacciani, L. 2019, MNRAS, 484, 2067
Sahakyan, N., Vardanyan, V., Giommi, P., et al. 2024, AJ, 168, 289
Sbarrato, T., Ghisellini, G., Tagliaferri, G., et al. 2015, MNRAS, 446, 2483
Sunyaev, R., Arefiev, V., Babyshkin, V., et al. 2021, A&A, 656, A132
Tavecchio, F., Maraschi, L., Ghisellini, G., et al. 2000, ApJ, 543, 535
Tramacere, A., Massaro, F., & Cavaliere, A. 2007, A&A, 466, 521
Tramacere, A., Massaro, E., & Taylor, A. M. 2011, ApJ, 739, 66
Traulsen, I., Schwope, A. D., Lamer, G., et al. 2020, A&A, 641, A137
Voges, W., Aschenbach, B., Boller, T., et al. 1999, A&A, 349, 389
Wakely, S. P., & Horan, D. 2008, in International Cosmic Ray Conference, 3, 1341
Webb, N. A., Coriat, M., Traulsen, I., et al. 2020, A&A, 641, A136
Zhao, X., Civano, F., Fornasini, F. M., et al. 2021, MNRAS, 508, 5176
Zhao, X., Civano, F., Willmer, C. N. A., et al. 2024, ApJ, 965, 188

Appendix A: Catalog of the 1007 sources without a 4FGL counterpart

Together with the paper, we make available the catalog of 1007 5BZCAT sources without 4FGL-DR4 counterpart and with at least an X-ray counterpart. These are the columns of the catalog.

- Column 1: 5BZCAT source ID, from Massaro et al. (2015).
- Column 2–3: Right Ascension (R.A.) and Declination (Dec) of the 5BZCAT source.
- Column 4: Source redshift, when available. From the 5BZCAT.
- Column 5: Object classification from the 5BZCAT (BZB, BZG, BZQ, or BZU): see Section 3 for a detailed description of each of these classifications.
- Column 6: Optical, R-band magnitude of the source, from the 5BZCAT. This is, as reported in the 5BZCAT catalog description, the "R-band magnitude of the blazar taken from the USNO-B1 Catalog, the r-band magnitude from SDSS DR10, or the magnitude in other bandpasses when these data are not available".
- Column 7: 1.4 GHz flux density of the source, from the 5BZCAT. This is, as reported in the 5BZCAT catalog description, the "radio flux density of the blazar at 1.4 GHz (from NVSS or FIRST), in mJy. Alternatively, if the 1.4 GHz flux density is not known, the flux density at 0.843 GHz from SUMSS is given".
- Columns 8–10: source ID, R.A., and Dec from the *XMM-Newton* 4XMM-DR13 X-ray catalog.
- Columns 11–13: source ID, R.A., and Dec from the *Chandra* 2CSC X-ray catalog.
- Columns 14–16: source ID, R.A., and Dec from the *Swift-XRT* 2SXPS X-ray catalog.
- Columns 17–19: source ID, R.A., and Dec from the eROSITA eRASS1 X-ray catalog.
- Columns 20–22: 0.2–12 keV observed X-ray flux and corresponding 90% confidence level lower and upper uncertainties, from the first catalog from which the source is detected, in this order: 4XMM-DR13, 2CSC, 2SXPS, eRASS1. For *Chandra*, *Swift-XRT*, and eROSITA the fluxes have been rescaled to the 0.2–12 keV band following the approach presented in Section 2.1.
- Column 23: 0.2–12 keV to 1.4 GHz flux ratio.
- Columns 24–25: Logarithm of the blazar SED synchrotron peak computed using the Blazar Synchrotron Tool, BlaST (Glauch et al. 2022).